

Robust Translational/Rotational Eye-Vergence Visual Servoing under Illumination Varieties

Hongzhi Tian, Yejun Kou, Khaing Win Phyu, Daiki Yamada and Mamoru Minami

Graduate school of Natural Science and Technology,

Okayama University, 3-1-1 Tsushima-naka, Kita-ku,

Okayama 700-8530, Japan

Email: {psnc8ytd, ptlg9dvi, p6nn3hpz, p7kw2h27}@s.okayama-u.ac.jp and minami-m@cc.okayama-u.ac.jp

Abstract—To track moving target, keep it at the center of the camera’s view and overcome the defects of fixed hand-eye visual servoing system, we proposed an eye-vergence visual servoing system. In the new system, left and right cameras’ directions could be rotated to observe and keep the target object to be seen at the center of camera images to reduce the influence of aberration of a camera lens. In practical applications among different indoor environments, lighting conditions may vary greatly. Therefore, the hue of HSV and model-based matching method are utilized to detect an object in the eye-vergence system. In this paper, it is carried out that comparison and analysis of recognition experiments in different illumination. Through the interior illumination changing experiment it can be ensured that the recognition method has a robustness to illumination changing within a certain range. And in the end, through a 3D pose tracking experiment, it can be verified that the tracking is still carried out smoothly even though illumination of object frequently changes.

I. INTRODUCTION

The visual servoing, a method for controlling a robot using visual information in the feedback loop, is expected to be able to allow the robot to adapt to changing or unknown environments [1]. Some methods have already been proposed to improve observation abilities by using stereo cameras [1], i.e., multiple cameras [3] or two cameras. There are two main configurations with stereo cameras, the first is an eye-in-hand configuration [2] that all cameras are mounted on the robot’s end-effector. The second configuration has the camera(s) fixed in the workspace [4]. These methods obtain multiple different views to observe an object by increasing the number of cameras.

As shown in Fig.1, the dual-eye stereo camera system is used in our eye-vergence visual servoing system [2]. The camera can rotate by itself. Therefore, the system can track a target to observe it at the center of camera images to enhance the tracking ability (trackability). In line with this tactic, the author has developed an eye-vergence visual servoing control system to enhance the trackability. About the superior 3D tracking performance under a single light environment we have described in detail [5], [6], [7]. And we have researched the performance of orientation recognition method[5].

There are other methods for identifying moving objects from a video sequence such as frame difference, background subtraction and optical flow three methods [8]. In a big class, there are many subclasses. For example, Lucas Kanade

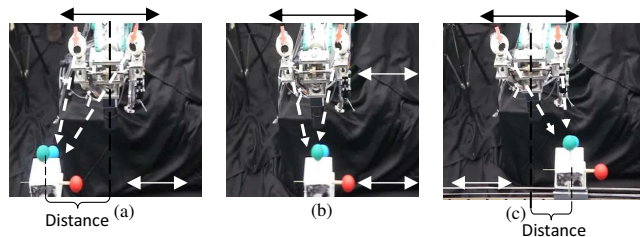


Fig. 1. For imitating the motion of human two cameras can rotate to gaze an object in the eye-vergence visual servoing system. The object is taking the horizontal reciprocating motion around the white arrow. And the end-effector is tracking it to keep facing it like (b). But the motion inertia of the manipulator is too large to track the object. Therefore, it is shown as (a) and (c), there is a distance between the object and end-effector. But the two cameras with the light moment of inertia can track the object in time. That is the merit of the eye-vergence visual servoing system.

pyramid optical flow are also fast enough and perform well in tacking tasks. However, they all need to compare two frames to detect an object. Our model-based matching method [9] is to solve detecting problems from another angle. It just directly process raw images and only the current ones. There is no need to compare pictures of different frames.

In this paper, the model construction is optimized and improved. We will research the indoor light environment adaptability of the proposed eye-vergence visual servoing system. Firstly we introduce the modeling method of a known object in detail. Secondly, as for detecting the object, a model-based matching method [9] is used. And genetic algorithm is utilized as an optimization algorithm to detected the object in real-time. The readers who are interested in modeling method and exploration method can read chapter II-A in detail.

This paper about eye-vergence visual servoing is basic research. Interested readers is referred to [10] for details about the application of the study.

II. 3D POSE TRACKING METHOD

A. Model-Based Recognition Using Real-Time Multi-Step GA

A 3D-ball-object as shown in Fig.5 (d) is used as 3D target object whose size and color are known.

Figure. 2 (a) shows searching models Σ_n without sampling points. The model to detect 3D-ball-object has the same 3D structure. The part of inner circle is named as S_{in} , and part between S_{in} and outer circle is named S_{out} . After a projection of the model to left and right images it will be shown as (b).

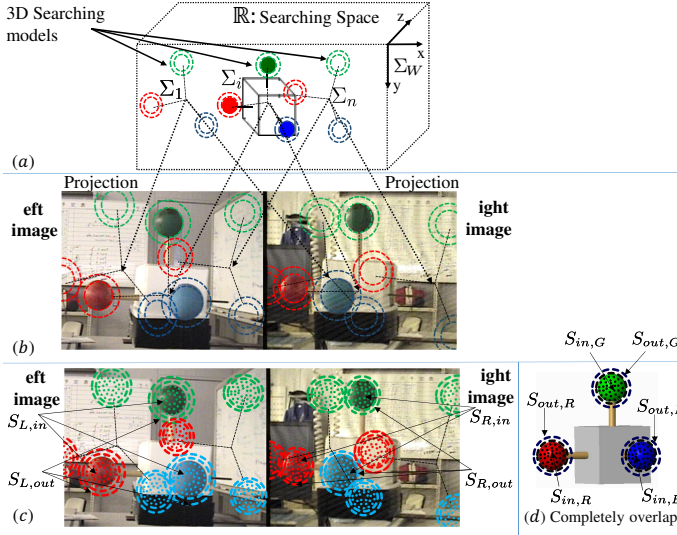


Fig. 2. Definition of a solid model without sampling points (a), left/right searching models after projection transformation (b) and taking sampling points in two images (c). When a model completely overlap the object (d), its fitness function gets the maximum

Then we take the sampling points on the images like (c) and calculate the fitness $F(E\psi_{\widehat{M}})$.

The dotted line block named \mathbb{R} in Fig.2 (a) means a searching space that will be described in detail in IV-B.

Through the projection transformation S_{in} and S_{out} are projected onto the 2D coordinates of left image Σ_{JL} and right image Σ_{JR} named S_L and S_R shown in Fig.2 (b).

As shown in Fig. 2 (d), inner portions of a model corresponding to three balls are $S_{in,R}, S_{in,G}$ and $S_{in,B}$. Similarly the three outer portions are $S_{out,R}, S_{out,G}$ and $S_{out,B}$. Each pair of circle and ring corresponds with a color, and three pairs of circles and rings are corresponding to red, blue and green. Each S_{in} is composed by three concentric circles with 36 sampling points. Each S_{out} is composed by two concentric circles with 24 sampling points. On each circle, 12 sampling points are taken at an equal interval. The sum of sampling points is

$$\Sigma_s = \Sigma_{sin} + \Sigma_{sout} = 3 \times (12 \times 3) + 3 \times (12 \times 2) = 180. \quad (1)$$

Hue information of HSV is used to search for the target object in the images. As shown of (3), as for a sampling point \mathbf{r}_i , its set hue value is H_u , i.e., $H_R = 0, H_G = 120, H_B = 240$. When $H_u - 20 < 0$ it will be replaced with $H_u - 20 + 360 > 0$. And the hue value of a pixel overlapped by \mathbf{r}_i is h_u . If h_u is near to H_u , the calculate value of \mathbf{r}_i is $p(\mathbf{r}_i) = 1$. Otherwise, $p(\mathbf{r}_i) = -1$. As shown of (4), the sum of $p(\mathbf{r}_i)$ of all the sampling points in a model Σ_i is defined as fitness $F(E\psi_{\widehat{M}})$. The value of a sampling point is shown as (3). The higher coincidence degree between a circle (inner portion) and corresponding color ball is, the higher fitness is. Conversely, the higher coincidence degree between a ring (outer portion) and the corresponding color ball is, lower fitness will be. When the searching model $\Sigma_{\widehat{M}}$ completely overlaps to the target

object like (d), then the fitness function gives maximum value

$$F_{max}(E\psi_{\widehat{M}}) = \Sigma_s / \Sigma_{sin} = 180 / 108 = 1.67. \quad (2)$$

When $F(C^L\psi_{\widehat{M}}) \leq 0$ or $F(C^R\psi_{\widehat{M}}) \leq 0$, it is set that $F(C^L\psi_{\widehat{M}}) = 0$ or $F(C^R\psi_{\widehat{M}}) = 0$

$$p(\mathbf{r}_i) = \begin{cases} 1 & (h_u \in [H_u - 20, H_u + 20], u = R, G, B), \\ -1 & (h_u \notin [H_u - 20, H_u + 20], u = R, G, B). \end{cases} \quad (3)$$

$$F(E\psi_{\widehat{M}}) = \left\{ \begin{aligned} & \left(\sum_{\substack{IR\mathbf{r}_i \in \\ S_{R,in}(C^R\psi_{\widehat{M}})}} p(IR\mathbf{r}_i) - \sum_{\substack{IR\mathbf{r}_i \in \\ S_{R,out}(C^R\psi_{\widehat{M}})}} p(IR\mathbf{r}_i) \right) / n_{R,in} \\ & + \left(\sum_{\substack{IL\mathbf{r}_i \in \\ S_{L,in}(C^L\psi_{\widehat{M}})}} p(IL\mathbf{r}_i) - \sum_{\substack{IL\mathbf{r}_i \in \\ S_{L,out}(C^L\psi_{\widehat{M}})}} p(IL\mathbf{r}_i) \right) / n_{L,in} \end{aligned} \right\} / 2 \\ = \{ F(C^R\psi_{\widehat{M}}) + F(C^L\psi_{\widehat{M}}) \} / 2 \quad (4)$$

To determine which solid model is most close to the real target, a correlation function used fitness function in Genetic Algorithm (GA) is defined for evaluation. This optimization problem is solved by GA. The i -th 3D model is represented by Σ_i , whose pose is assumed to the defined by chromosome

$$\underbrace{10 \dots 10}_{12bit} \underbrace{11 \dots 01}_{12bit} \underbrace{01 \dots 10}_{12bit} \underbrace{11 \dots 10}_{12bit} \underbrace{10 \dots 10}_{12bit} \underbrace{10 \dots 01}_{12bit}.$$

Detail discussion about Real-Time Multi-Step GA (RT-MS GA) is explained in [9], [10].

B. Orientation Recognition Method Using Quaternion

In our system quaternion representation [11] has been adopted. The definition of unit quaternion is shown in Fig.3. On the basis of axis-angle representation, a unit vector \mathbf{k} indicating direction, and an angle θ describing the magnitude of rotation around the axis. By using \mathbf{k} and θ , quaternion set $\mathbf{q} = \{\eta, \varepsilon\}$, \mathbf{q} is defined as follows,

$$\varepsilon = [\varepsilon_1, \varepsilon_2, \varepsilon_3]^T = [k_x, k_y, k_z]^T = \sin \frac{\theta}{2} \mathbf{k}, \quad (5)$$

η is the scalar part of the quaternion, and ε is the vector part of the quaternion. They satisfy the following relationship of unit quaternion:

$$\eta^2 + \varepsilon^T \varepsilon = 1. \quad (6)$$

III. HAND & EYE VISUAL SERVOING CONTROLLER

The block diagram of our proposed hand & eye-vergence visual servoing controller is shown in Fig.4.

The manipulator is 7 links, each joint angle is set to $\mathbf{q}_H = [q_1, \dots, q_7]$. And the end-effector has 6-DOF, so q_1 is set as 0 to remove the redundancy of the robot PA 10. The desired angle of each link is set to \mathbf{q}_{Hd} . For camera system, $\mathbf{q}_C =$

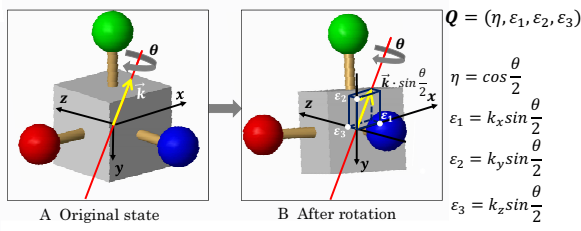


Fig. 3. Definition of quaternion in the proposed system

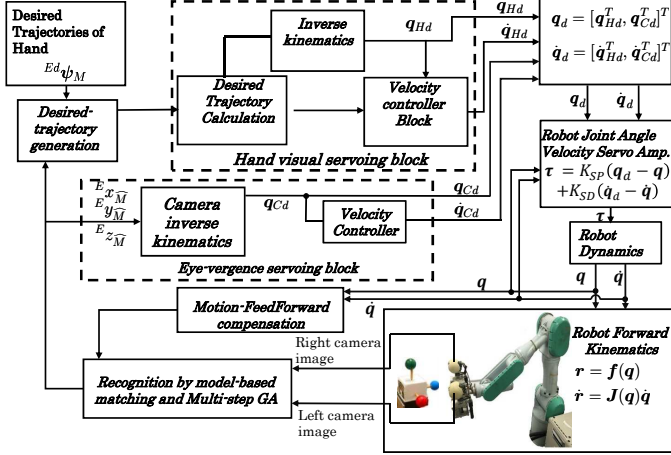


Fig. 4. Block diagram of the hand visual servoing system

$[q_8, q_9, q_{10}]$, and q_8 is tilt angle, q_9 and q_{10} are pan angles. The desired angle of q_C is set to $q_{Cd} = [q_{8d}, q_{9d}, q_{10d}]$.

In Fig.4, the hardware control system of the velocity-based servo system of PA10 is expressed as

$$\tau = K_{SP}(q_d - q) + K_{SD}(\dot{q}_d - \dot{q}) \quad (7)$$

where K_{SP} and K_{SD} are symmetric positive definite matrices to determine PD gain. The controller of eye-visual servoing is given by

$$\dot{q}_{id} = K_P(q_{id} - q_i) \quad (i = 8, 9, 10) \quad (8)$$

where K_P is spring constant. \dot{q}_{id} is input into pulse motors for the cameras' angles control as a pulse array.

IV. EXPERIMENT OF HAND & EYE-VERGENCE VISUAL SERVOING

A. Experimental System

The utilized manipulator in the system is PA-10 robot arm manufactured by Mitsubishi Heavy Industries. And two rotatable cameras mounted on the end-effector are FCB-1X11A manufactured by Sony Industries. The frame frequency of stereo cameras is set as 30fps. The image processing board, CT-3001, receiving the image from the CCD camera is connected to the host computer (CPU: Intel Core i7-3770, 3.40 GHz). The structure of the manipulator and the cameras are shown in Fig.5.

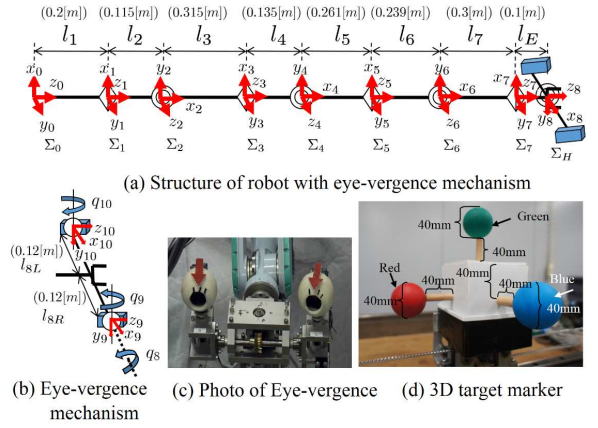


Fig. 5. Frame structure of manipulator

B. Interior Illumination Changing Experiment

Figure 6 shows the search area of GA that is defined based on the range of motion of the object. Target position and orientation relationship between the object and the end-effector is set as:

$$E_d \psi_M = [0, -100[mm], 545[mm], 0, 0, 0]. \quad (9)$$

If the range of exploration is too large, this will increase the difficulty of convergence of GA to tracking objects and the amount of unnecessary calculations. That is, the time required for the algorithm becomes longer from the calculation start to the termination criteria. This is unacceptable for a real-time tracking system. If the search range is too small, the object may be outside the search range.

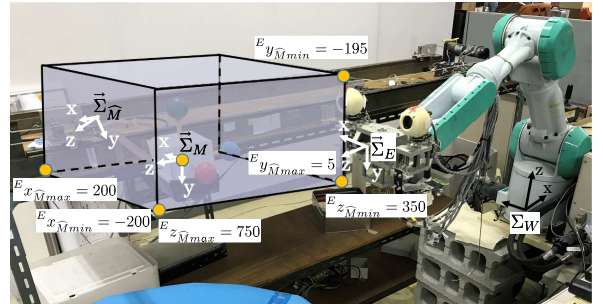


Fig. 6. Search area of GA. The origin of object generated randomly by GA is limited to only in the area shown in the figure. The true object is $\hat{\Sigma}_M$. A detected position of the target object is $E_x \hat{M} \in [-200, 200]$, $E_y \hat{M} \in [-195, 5]$, $E_z \hat{M} \in [350, 750]$

According to pre-set tracking conditions of (9) and a number of tests, as shown in Fig.4 and Fig.6, we set the search area of GA as

$$E_x \hat{M} \in [-200, 200], E_y \hat{M} \in [-195, 5], E_z \hat{M} \in [350, 750]. \quad (10)$$

where unit is [mm].

1) *Symbol Meaning*: M represents the object and \hat{M} represents the estimated object. Then $\vec{\Sigma}_M$ denotes the coordinate system that moves along with the object.

In the figure $\vec{\Sigma}$ represents a coordinate system moving in the world coordinate system Σ_W . The coordinate system

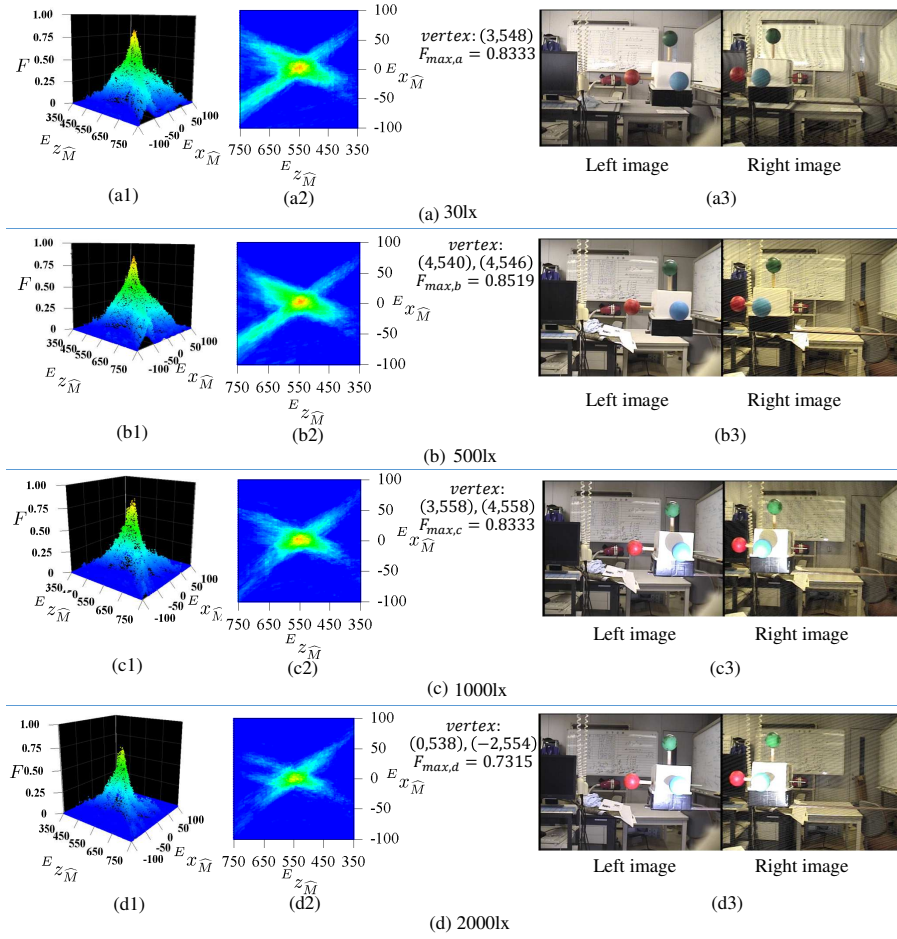


Fig. 7. Illumination changing and background changing experiment. (a)~(d) show the results of experiments with different illumination. (a3)~(d3) show the left and right images in each experiment. (a1)~(d1) show the distribution of fitness on each point on $E x_M - E z_M$ plane in search area. Exploration interval is 1[mm], i.e. $E x_M = -100, -99, \dots, 99, 100$; $E z_M = 350, 351, \dots, 749, 750$. (a2)~(d2) are the 2D figure of (a1)~(d1). In each experiment, “vertex” show the position $(E x_M, E z_M)$ with maximum fitness F_{max} .

represented by Σ keeps fixed in Σ_W . In other words $\vec{\Sigma}_E, \vec{\Sigma}_M, \vec{\Sigma}_{CL}, \vec{\Sigma}_{CR}$ and $\vec{\Sigma}_M$ are all moving in Σ_W . On the other hand, as shown in Fig.8, Σ_B keeps fixed in the world coordinate system Σ_W .

As shown in Fig. 6, the position and orientation of the object Σ_M and the end-effector $\vec{\Sigma}_E$ are unchanged in each group of experiments. And the relative position of Σ_M and $\vec{\Sigma}_E$ is $E \mathbf{r}_M = (0, -100, 545)$. And their orientations are same, i.e., $W \boldsymbol{\varepsilon}_M = W \boldsymbol{\varepsilon}_E = (0, 0, 0)$.

Figure 7 shows the results of recognition in different illumination conditions. The images on the right side of each row are taken by the two cameras in different experimental conditions. In (a)~(d), only the illumination is changed, the object and the arm are not moved.

The left two columns ($a_1 \sim d_1$ and $a_2 \sim d_2$) of Fig. 7 are fitness distributions in $E x_M - E z_M$ plane under different experimental conditions. The distribution of the middle column ($a_2 \sim d_2$) is the 2D display of the leftmost fitness distribution ($a_1 \sim d_1$).

For example, in the row (b), the two images are taken in 500[lx]. In the case of given true values $E \boldsymbol{\varepsilon}_M = E \boldsymbol{\varepsilon}_E =$

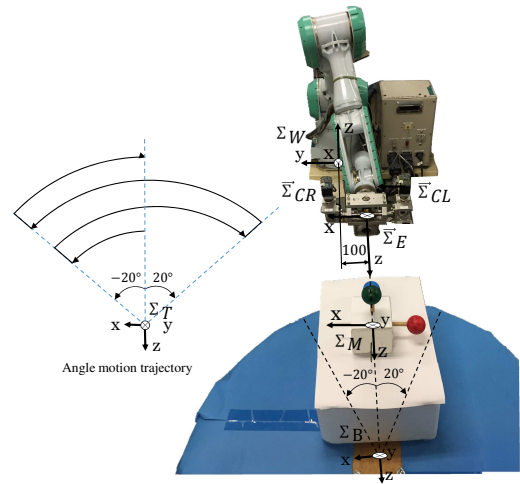


Fig. 8. Distribution of the initial state of each coordinate system and the angle motion trajectory

$0, {}^E y_{\widehat{M}} = {}^E y_M = -100$, the target object is searched on the ${}^E x - {}^E z$ plane. And the fitness distribution is shown as Fig. 7 (b1). The (b2) is a 2D figure of (b1). There are two highest points (vertex), i.e., the peak of the mountain of the distribution. One is ${}^E x_{1\widehat{M}}, {}^E z_{1\widehat{M}} = (4, 540)$. And the other is ${}^E x_{2\widehat{M}}, {}^E z_{2\widehat{M}} = (4, 546)$. That means, according to the model-based matching method, object is most likely to be in either $({}^E r_{1\widehat{M}}, {}^E \varepsilon_{1\widehat{M}}) = (4, -100, 540, 0, 0, 0)$ or $({}^E r_{2\widehat{M}}, {}^E \varepsilon_{2\widehat{M}}) = (4, -100, 546, 0, 0, 0)$ with fitness value $F_1 = F_2 = F_{max,b} = 0.8519$. It can be seen that they are near to the true value. In order to quickly find the vertex of the mountain (maximum), we use the RT-MS GA described in II-A. However, it should be noted that the full search on the ${}^E x - {}^E z$ plane of these experiments just detect only the x and z two variables. In the actual object tracking experiment it is needed to detect position and orientation 6 variables, i.e. ${}^E \psi_{\widehat{M}} = ({}^E x_{\widehat{M}}, {}^E y_{\widehat{M}}, {}^E z_{\widehat{M}}, {}^E \varepsilon_{\widehat{M}1}, {}^E \varepsilon_{\widehat{M}2}, {}^E \varepsilon_{\widehat{M}3})$.

In (a) the illumination 30[lx] is too low that there are more black points than (b). Therefore, the $F_{max,a} > F_{max,b}$. (b) ~ (d) the illumination is gradually increasing. And there are more and more white points in the images. Therefore, $F_{max,b} > F_{max,c} > F_{max,d}$.

C. Arc Swing Motion Tracking Experiment under Different Light Condition

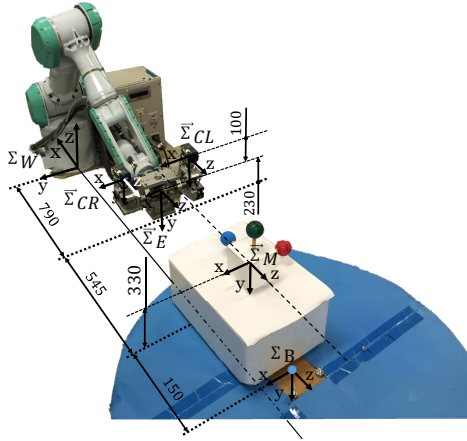


Fig. 9. Distribution of the initial state of object and visual-servoing system in orientation tracing experiment

1) *Experiment condition:* As shown in Fig.9, in the process of tracking, always keep the x-y plane in $\vec{\Sigma}_E$ parallel to the x-y plane in $\vec{\Sigma}_M$. Σ_B is the coordinate system of turntable. And the turntable takes $\pm 20^\circ$ reciprocal uniform rotation movement around y-axis of Σ_B .

At this speed it takes 80s to rotate one cycle, that means the angular velocity $\omega = \pm 2\pi/T = \pm 2\pi/80 = \pm 0.079[\text{rad/s}]$.

During the experiment we just let object rotate around the y-axis of Σ_B as (12), the orientation ε_M of object is

$$[\varepsilon_{M1}, \varepsilon_{M2}, \varepsilon_{M3}]^T = \sin \frac{\theta}{2} [0, 1, 0]^T = [0, \sin \frac{\theta}{2}, 0]^T \quad (11)$$

shown as the dashed line in the Fig.11. In this light changing experiment, the illumination condition is divided into 80[lx],

500[lx], 900[lx], and 2200[lx] four cases. Because turntable takes the reciprocating motion, (12) can be rewritten as periodic function with period $T_a = 4 \times 4.44 = 17.76[\text{s}]$. Therefore, the equation $\theta(t) = \theta(t + 17.76)$ holds. And in the first period, the $\theta(t)$ is shown as follow.

$$\theta(t) = \begin{cases} -4.5t & t \in [0, 4.44)s & (12a) \\ 4.5t - 40 & t \in [4.44, 13.32)s & (12b) \\ -4.5t + 80 & t \in [13.32, 17.76)s & (12c) \end{cases}$$

2) *Experimental Result:* As shown in Fig. 11, (a) is fitness value during the tracking process calculated by (4). It shows at each time the degree of matching between the object and the best individual evolved from GA. As described in section II-A, the maximum of fitness is $F_{max} = 1.67$. The fitness can be affected by many factors, e.g., the quality of the captured images, the motion of manipulator or the changing of light. In Fig. 11 (a) because the fitness takes dramatic fluctuations it can be seen that changes in light illumination affect the object recognition.

Fig. 10 shows the experiment situation. The subtitle of each picture, e.g., 5[s], 36[s], is the photograph time corresponding to the time in Fig. 11. Left and right images are captured by the two cameras. And the light point circles are the recognition result at that time. In Fig. 11 (b), the dashed lines represent the orientation ε_M of real target $\vec{\Sigma}_M$. Orientation tracking result of the detected object $\vec{\Sigma}_{\widehat{M}}$ and end-effector $\vec{\Sigma}_E$ are shown as the solid line $\varepsilon_{\widehat{M}}$ and dotted line $\varepsilon_{\widehat{E}}$ respectively.

Fig. 11 (c) shows the tracking error of hand $\Delta \varepsilon_{EM2}$ and GA $\Delta \varepsilon_{M\widehat{M}2}$. And as shown in Fig. 11 (b), the desired value of ε_2 of hand ε_{E2} and object $\varepsilon_{\widehat{M}2}$ is ε_{M2} , i.e., the triangular wave in dashed line. The quaternion variation of $\varepsilon_{\widehat{M}}$ is more frequent than that of ε_E . In Fig. 11 the phases of $\varepsilon_{\widehat{M}2}$ are all earlier than that of $\vec{\Sigma}_E$.

Another point that can be confirmed is that although the fitness is changed a lot because of the illumination changing, the recognition result and the motion of manipulator was not influenced so much. It shows that the system can overcome some illumination change and keep track the target. Although at about 32[s], there is a transient error in orientation detection. But because the time is very short and the system is slow to respond, the error does not cause much influence to the tracking motion.

V. CONCLUSION

In order to evaluate the adaptability to the light environment, it has been designed that the interior illumination changing experiment and arc swing motion tracking experiment. Through these experiments, it has been verified that the proposed eye-vergence visual servoing system has the robustness against the changeable optical environment. Need to be reminded that the proposed system is developed for the interior illumination environment. In the sunny outdoor, the illumination has more than 30,000[lx], this is not within our scope of the investigation. In addition, a reflectivity of an object itself will also affect the object recognition. A camera's auto exposure

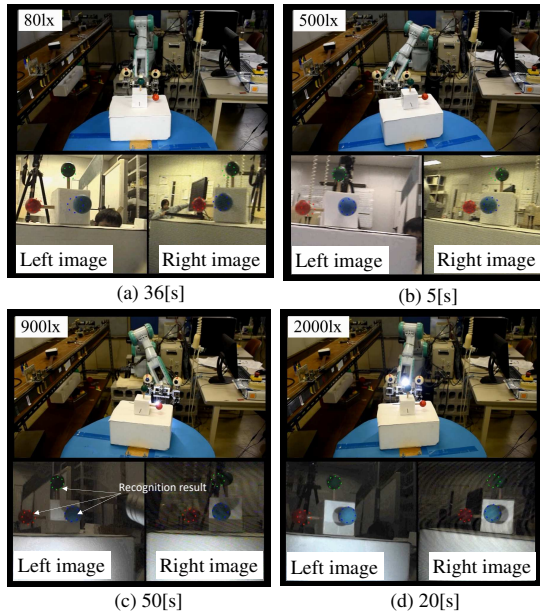


Fig. 10. The experimental status and dual-eye images under different illuminations. The upper left corner of each picture is marked with the current illumination. And the subtitle of each picture is the photography time corresponding to the time in Fig.11

function also affects the quality of the collected images. These factors have not been explored in this paper. Further research will be conducted in the relevant aspects in the future.

REFERENCES

- [1] Hutchinson, Seth, Gregory D. Hager, and Peter I. Corke. "A tutorial on visual servo control." *Robotics and Automation, IEEE Transactions on* 12.5, pp. 651-670, 1996.
- [2] Song, Wei, Mamoru Minami, Yasushi Mae, and Seiji Aoyagi. "On-line evolutionary head pose measurement by feedforward stereo model matching." In *Robotics and Automation, 2007 IEEE International Conference on*, pp. 4394-4400. IEEE, 2007.
- [3] Stavnitzyk, Jay, and David Capson. "Multiple camera model-based 3-D visual servo." *Robotics and Automation, IEEE Transactions on* 16.6, pp. 732-739, 2000.
- [4] Dune, Claire, Eric Marchand, and Christophe Leroux. "One click focus with eye-in-hand/eye-to-hand cooperation." In *Robotics and Automation, 2007 IEEE International Conference on*, pp. 2471-2476. IEEE, 2007.
- [5] Tian, Hongzhi, Ryuki Funakubo, Yejun Kou, and Mamoru Minami. "3D evolutionary pose tracking experiments of eye-vergence visual servoing in lateral motion and arc swing motion." In *Robotics and Biomimetics (ROBIO), 2016 IEEE International Conference on*, pp. 577-582. IEEE, 2016.
- [6] Nishimura, Kenta, Sen Hou, Koichi Maeda, Mamoru Minami, and Akira Yanou. "Analyses on on-line evolutionary optimization performance for pose tracking while eye-vergence visual servoing." In *2013 IEEE International Conference on Mechatronics and Automation*, pp. 698-703. IEEE, 2013.
- [7] Tian, Hongzhi, Yu Cui, Mamoru Minami, and Akira Yanou. "Frequency response experiments of eye-vergence visual servoing in lateral motion with 3D evolutionary pose tracking." *Artificial Life and Robotics* 22, no. 1 (2017): 36-43.

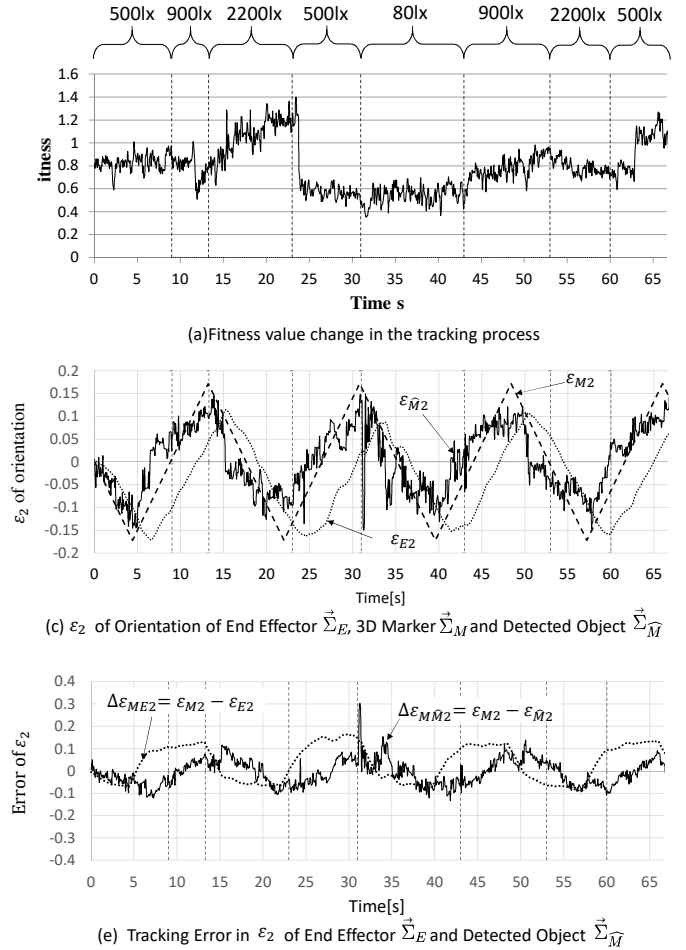


Fig. 11. Tracking result under different illumination. Actual orientation of target object ε_M , actual position of end-effector ε_E and detected orientation recognized by GA $\varepsilon_{\hat{M}}$. In ε_2 direction, tracking error of end-effector (hand) is $\Delta\varepsilon_{EM2}$ and recognition error is $\Delta\varepsilon_{M\hat{M}2}$.

- [8] Cucchiara, Rita, C. Grana, Metal Piccardi, and A. Prati. "Statistic and knowledge-based moving object detection in traffic scenes." In *Intelligent Transportation Systems, 2000. Proceedings. 2000 IEEE*, pp. 27-32. IEEE, 2000.
- [9] Myint, Myo, Mamoru Minami, Kenta Yonemori, Khin Lwin, Akira Yanou, "Dual-eyes Visual-based Sea Docking for Sea Bottom Battery Recharging." *MTS/IEEE OCEANS' 16*, September 19-23, 2016.
- [10] Myint, Myo, Kenta Yonemori, Akira Yanou, Khin Nwe Lwin, Mamoru Minami, and Shintaro Ishiyama. "Visual Servoing for Underwater Vehicle Using Dual-Eyes Evolutionary Real-Time Pose Tracking." *Journal of Robotics and Mechatronics* 28, no. 4, pp. 543, 2016.
- [11] Song, Wei, Mamoru Minami, and Seiji Aoyagi. "On-line stable evolutionary recognition based on unit quaternion representation by motion-feedforward compensation." *International Journal of Intelligent Computing in Medical Sciences & Image Processing* 2.2, pp. 127-139, 2008.
- [12] Maeda, Koichi, Mamoru Minami, Akira Yanou, Hiroaki Matsumoto, Fujia Yu, and Sen Hou. "Frequency response experiments of 3-d pose full-tracking visual servoing with eye-vergence hand-eye robot system." In *SICE Annual Conference (SICE), 2012 Proceedings of*, pp. 101-107. IEEE, 2012.